GeoConvention 2015
GEOSCIENCE
new horizons
Telus Convention Centre • 4-8 May 2015 • Calgary, AB Canada

Ultrasonic Investigation of Elastic Anisotropy in Duvernay Shales

Oliver N. Ong[1], Douglas R. Schmitt[1], Randolf Kofman[1], and Kristine Haug[2]
[1]Institute for Geophysical Research – University of Alberta
[2]Alberta Energy Regulator – Alberta Geological Survey

Summary

Laboratory measurements of anisotropy in shales have been increasingly important in hydrocarbon exploration as focus shifts from conventional reservoirs to shale-gas reservoirs. In this study, the elastic properties of Duvernay shales are investigated through ultrasonic measurements on core samples. Results show that the material is of a vertical transverse isotropic nature with observations showing a greater stiffness parallel to the foliation plane. Study of the dynamic elastic moduli yields evidence that the greater source of anisotropy within the sample is due to intrinsic properties such as the preferential alignment of minerals and fine sediment layering.

Introduction

Elastic anisotropy is defined as a variation of wavespeed as a function of its propagation direction within a medium. The understanding of the directional dependence of seismic waves have become increasingly important in the context of rock mechanics and signal processing as interest in unconventional reservoirs increases (Hornby, et al., 1994; Banik, et al., 2012). Shales exhibit a relatively large degree of anisotropy as microcracks, fractures, preferential clay mineral alignment, and layering all contribute to this phenomenon. In this study, the elastic properties of Duvernay shales are investigated through the use of ultrasonic velocity measurements. Samples are assumed to be transversely isotropic with a vertical axis of symmetry and with this assumption, static and dynamic elastic moduli are calculated and compared to provide insight into the properties of these samples. Here, we outline the methodology used and provide some preliminary results.

Theory and/or Method

In order to investigate the degree of anisotropy in these samples, the 5 independent elastic constants that describe the elastic stiffness matrix are calculated from a minimum of 5 phase velocities. These velocities are determined through the use of piezoelectric ceramic transducers in the Pulse Transmission Method (Kebaili, 1997; Hemsing, 2007; Melendez & Schmitt, 2011). These P-wave and S-wave transducers are capable of creating an impulse with the application of an electric potential and producing said electric potential when experiencing an mechanical disturbance. With known offset between the transducers, the phase velociy can be calculated as a simple ratio of the travel time and distance traveled.

P and S-wave velocities are calculated in the orientations perpendicular ($V_p(0°)$, $V_{SH}(0°)$), parallel ($V_p(90°)$, $V_{SH}(90°)$), and 45° (($V_p(45°)$, $V_{SV}(45°)$) to the foliation plane. The sample is trimmed into a prism-like geometry using diamond-tipped circular saw with each face ground parallel using a grinding wheel. The entire surface of the sample is then polished with fine-grain sandpaper to ensure proper cohesion of the transducers. This configuration, adapted from Melendez (2014) allows us to overcome the hetergeneity issues of measuring the velocities through mulitple cores.

The setup consists of copper pads epoxied directly onto the faces of the sample to act as a common ground for each transducer pair. The transducers themselves are then glued onto the copper pads using a silver conductive epoxy with another small copper piece on top to act as the positive electrode. In addition to the transducers, linear strain gauges are mounted onto the sample measuring the deformation parallel and perpendicular to bedding. To finish the setup, wires are soldered onto the positive and negative electodes as well as the strain gauges. The entire sample is then covered in a non-conductive urethane compound (Devcon Flexane ® 80) to prevent contamination of the sample by the confining fluid of the pressure vessel. The sample is then placed into the pressure vessel and wires are fed through to a setup consisting of an oscilloscope, power supply, pulser, and digitizer.

Travel times are picked from the first extremum of an averaged waveform stacked approximately 300 times to reduce the random noise of the signal. P and S-wave velocities are calculated for the pressurization and depressurization cycle for the full range of 0 – 90 MPa.

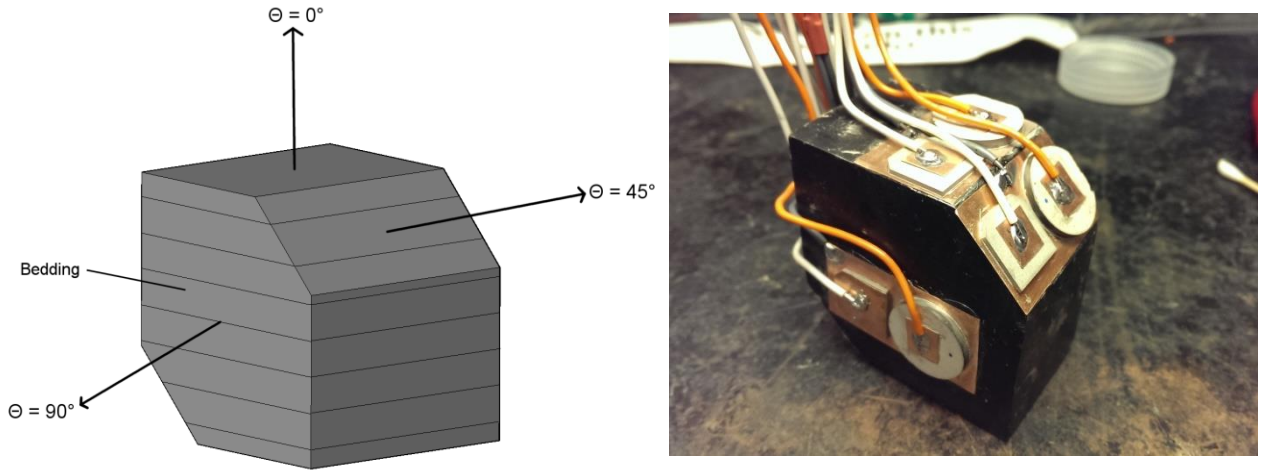

Figure 1. Model of the sample showing transmission orientations (left) and picture of finished sample before application of Flexane

Examples

In this section, phase velocities as well as estimations of the static and dynamic moduli are shown as preliminary results of the ultrasonic measurements. Figure 2 plots the phase velocities as a function of confining pressure where the arrows show the progression of measurements in the pressurization and depressurization cycle.

The observations are consistent with what we would expect from a material with vertical transverse isotropic symmetry where $\boldsymbol{V_P(0°) < V_P(45°) < V_P(90°)}$, and $\boldsymbol{V_{SH}(0°) < V_{SV}(45°) < V_{SH}(90°)}$. As a general trend, all velocities increase with confining pressure as the sample becomes stiffer due to the closure of microcracks, fractures, and other void space within the material. As a result, the anisotropy in the sample also decreases with confining pressure, though large differences in velocity at high pressures tell us that these microcracks and fractures only account for a small source of anisotropy.

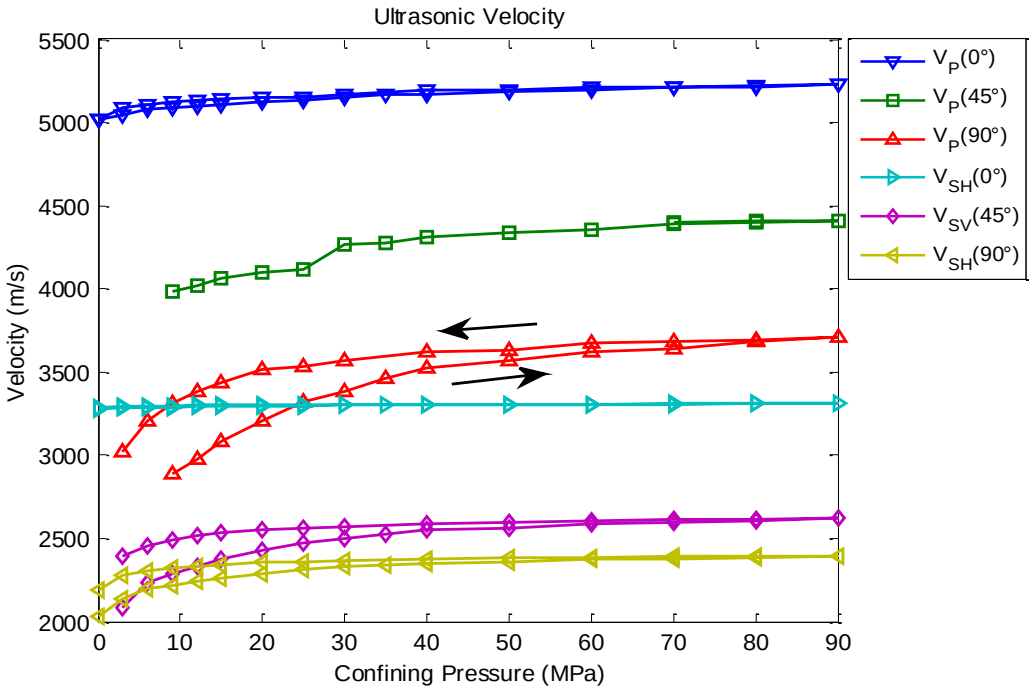

Figure 2. P-wave and S-wave velocities plotted as a function of confining pressure. Arrows show progression of measurements

In addition, hysteresis effects are observed for all velocities due to the microcracks closing at a faster rate during pressurization than opening during depressurization **(Hemsing, 2007)**. Figure 3 plots the dynamic Young's modulus and Poisson's ratio as a function of confining pressure.

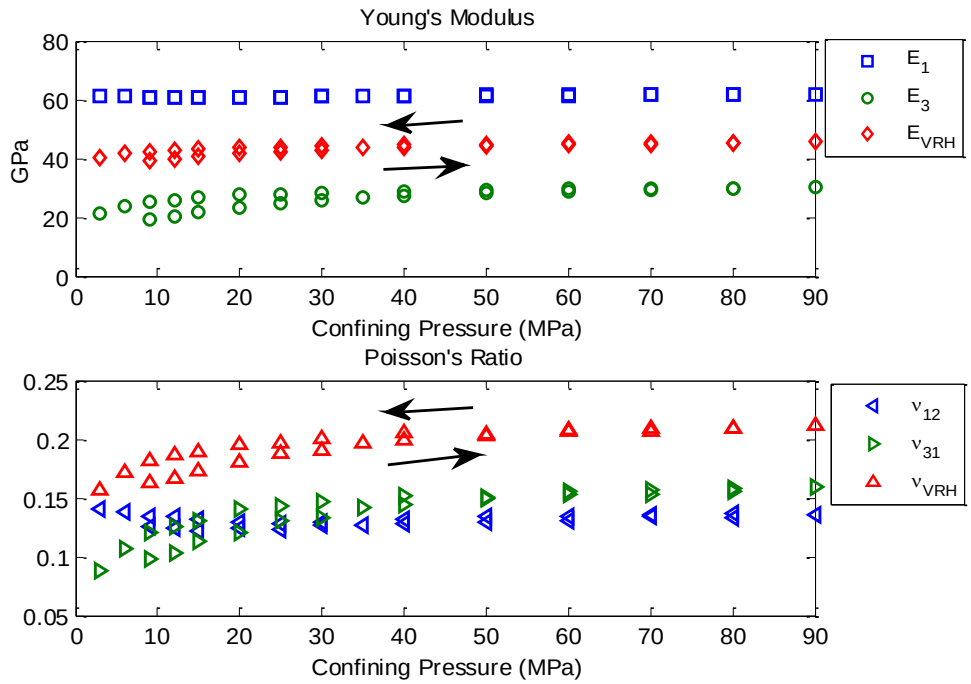

Figure 3. Dynamic Young's modulus and Poisson's ratio plotted as a function of confining pressure

where the subscript *VRH* is the Voigt-Reuss-Hill approximation (average of Voigt and Reuss bounds) of the moduli assuming an isotropic polycrystalline aggregate. All other moduli are calculated under the assumption of an anisotropic single crystal where the numerical subscripts represent one of the orthogonal directions. The inequality of Young's modulus shows that the sample is stiffer in the direction parallel to bedding than perpendicular to bedding. Sayers (2013) noted that ν_{12} can be greater than, equal to, or less than ν_{31}. Results have shown that an inequality of $\nu_{12} > \nu_{31}$ at low pressures may indicate the presence of microcracks where as at high pressures, $\nu_{31} > \nu_{12}$ can be attributed to preferential alignment of clay minerals. Our observations are consistent with this statement.

Figure 4 plots the dynamic bulk modulus assuming both an anisotropic single crystal and an isotropic polycrystalline aggregate. The static tangent bulk modulus is also calculated from a regression fitted to the stress-strain relationship.

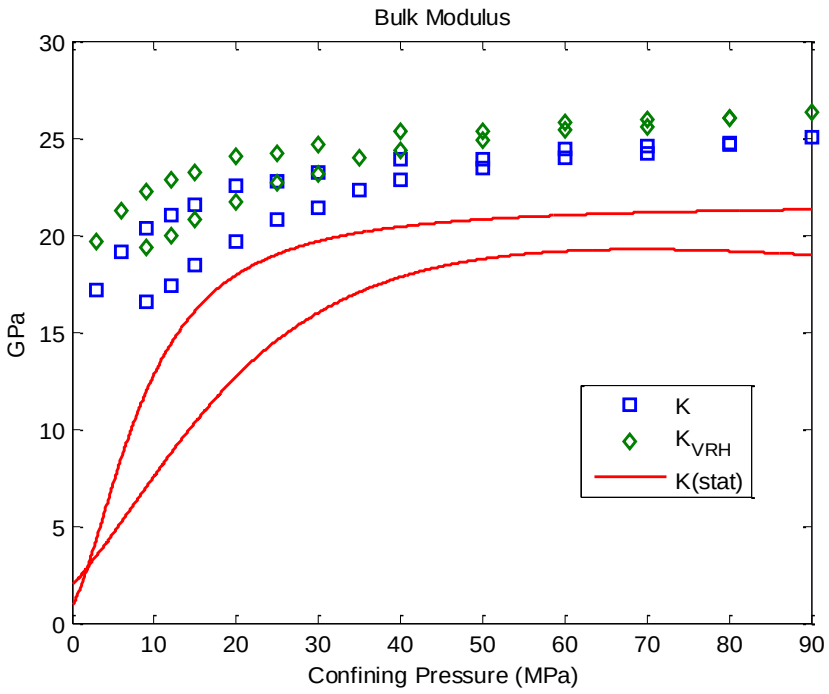

Figure 4. Comparison of static and dynamic bulk moduli plotted as a function of confining pressure

Conclusions

The preliminary results from the ultrasonic velocity measurements are consistent with the results we would expect from a material with vertical transverse isotropy. Velocity increases with increasing confining pressure as the sample becomes stiffer as a result of microcracks and fractures closing. At high pressures, the large remaining discrepancy between the velocity values indicate that the largest source of anisotropy in the sample is most likely due to intrinsic properties such as preferential mineral alignment and fine layering of sediments (Johnston & Christensen, 1995; Backus, 1962). Hysteresis effects are observed in all measurements in the pressurization and depressurization cycles.

Acknowledgements

We would like to thank the University of Alberta and the Natural Sciences and Engineering Research Council of Canada (NSERC) for their generous support. We would also like to thank the Alberta Geology Survey for providing the core samples needed for this study.

References

Backus, G. E., 1962. Long-wave Elastic Anisotropy Produced by Horizontal Layering. *Journal of Geophysical Research ,* 67(11), pp. 4427-4440.

Banik, N., SPE, Egan, M. & Schlumberger-WesternGeco, 2012. *Effects of VTI Anisotropy of Shale Reservoir Characterization.* Abu Dhabi, UAE, Society of Petroleum Engineers.

Hemsing, D. B., 2007. *Laboratory determination of seismic anisotropy in sedimentary rock from the Western Canadian Sedimentary Basin,* Edmonton, AB: University of Alberta.

Hornby, B. E., Schwartz, L. M. & Hudson, J. A., 1994. Anisotropy effective-medium modeling of the elastic properties of shales. *Geophysics.*

Johnston, J. E. & Christensen, N. I., 1995. Seismic anisotropy of shales. *Journal of Geophysical Research,* 100(B4), pp. 5991-6003.

Kebaili, A., 1997. *Velocity anisotropy determination in tau-p space,* Edmonton, AB: Geophysics.

Melendez, J., 2014. *Elastic Properties of Sedimentary Rocks,* Edmonton, AB: University of Alberta.

Melendez, J. M. & Schmitt, D. R., 2011. Investigating anisotropy in rocks by using pulse transmision method. *CSEG Recorder,* 36(10), pp. 34-38.

Sayers, C. M., 2013. The effect of anisotropy on the Young's moduli and Poisson's ratios of shales. *Geophysical Prospecting ,* 61(2), pp. 416 - 426.